

PREPARATION OF ZINC OXIDE AND POLY-ETHYLENE OXIDE COMPOSITE MEMBRANES AND THEIR PHASE RELATIONSHIP

PREPARACIÓN Y RELACIÓN DE FASES DE MEMBRANAS DEL COMPOSITO DE OXIDO DE ZINC Y POLY-ETHYLENE

JESÚS FABIAN JURADO

Ph.D. Universidad Nacional de Colombia, Sede Manizales, jffurado@unal.edu.co

CARLOS VARGAS HERNÁNDEZ

Ph.D. Universidad Nacional de Colombia, Sede Manizales, cvargash@unal.edu.co

RUBÉN ANTONIO VARGAS

Ph.D. Universidad del Valle, Cali, Colombia, ruben.vargas@correounivalle.edu.co

Received for review November 4th, 2011, accepted April 3th, 2012, final version May, 3th, 2012

ABSTRACT: Zinc oxide and organic polymer (poly-ethylene oxide) based nanocomposite membranes were prepared and their phase relationship investigated. The composites were characterized by XRD, Raman scattering, DSC, and impedance spectroscopy analysis. It was found that embedding inorganic nanoparticles of ZnO into the polymer matrix of PEO allowed for some crystallinity formation, and cross-linking of the polymer composites during annealing or synthesis. The XRD and Raman scattering results show more defined peaks assigned to each phase of the composite as the ZnO content increases from 0 to 30% weight ratio, thus indicating that ceramic filler remain in the semi-crystalline polymer matrix as a separate crystalline phase. The dc-electrical conductivity increases by two or three orders of magnitude from blank (organic phase only) ($\sim 10^{-6} \text{ Scm}^{-1}$) to the 30 % wt. ZnO composite membrane ($\sim 10^{-4} \text{ Scm}^{-1}$). Electrical conduction changed as a function of temperature with an Arrhenius-type behavior.

KEYWORDS: Poly-ethylene oxide (PEO), Composite materials, Raman scattering, Polyelectrolytes, Dielectric properties.

RESUMEN: El compuesto polimérico tipo membrana de óxido de zinc con el polímero orgánico poly(ethylene)oxide, fue manufacturado para estudiar la correlación de fases. Difracción de rayos-X (XRD), Dispersión Raman (RS) calorimetría diferencial de barrido (DSC) y espectroscopia de impedancia (EI) mostraron que las nano-partículas de ZnO están inmersas homogéneamente en la matriz de PEO dándole un cierto orden cristalino. Las posiciones de los picos de los registros XRD y RS del composito evidenciaron la separación de la fase semi-cristalina de PEO con la fase cristalina del ZnO para todo el rango del contenido. La variación de la conductividad eléctrica dc con la temperatura es tipo Arrhenius para el composito. La conductividad eléctrica dc del PEO ($\sim 10^{-6} \text{ Scm}^{-1}$) se incrementa en cerca de dos órdenes de magnitud con la presencia 30% wt. de ZnO ($\sim 10^{-4} \text{ Scm}^{-1}$).

PALABRAS CLAVE: Poly-ethylene oxide (PEO), Materiales composito, Espectroscopia Raman, Poliméricos electrolíticos, Propiedades dieléctricas.

1. INTRODUCTION

Permanent electrical effects in polymer-based materials have been utilized in a wide variety of applications and have steadily gained growing importance in our daily life. These extend from technological areas to the biological and medical fields and have impact in various areas of research, development, or production. The study of electrical conductivity behavior constitutes a powerful approach for obtaining information about the nature and types of molecular motions and the manner

in which they are affected by chemical composition, molecular structure, and morphology [1–4].

Numerous investigations have been conducted on a variety of polymeric composites with an aim to understand the nature [5,6] of complexation and to characterize the obtained materials. The main advantages of PEO as a matrix polymer are its chemical, mechanical, and electrochemical stabilities, since it contains only strong unstrained C–O, C–C, and C–H bonds. PEO shows the glass transition temperature

at $T_g = 61$ °C and crystalline melting in the region between 50° and 70 °C. PEO is very flexible because of the presence of swivel ether linkages and the repeat unit, $-\text{CH}_2\text{CH}_2\text{O}-$, provides just the right spacing to accommodate other atomic species.

ZnO is a wide band gap semiconductor with great potential for a variety of commercial applications. The native doping of the semiconductor (due to oxygen vacancies) is n-type. This semiconductor has several favorable properties: good transparency, high electron mobility, wide bandgap, strong room-temperature luminescence, etc. Those properties are already used in emerging applications for transparent electrodes in liquid crystal displays and in energy-saving or heat-protecting windows, and electronic applications of ZnO as thin-film transistors and light-emitting diodes. Zinc oxide nanoparticles (ZnO) have become one of the most widely-studied metal oxide materials [7]. The tremendous interest is provoked by the multifunctional characteristics of ZnO and various options to tune its properties by controlling size and morphology. As a white powder, ZnO finds extensive use today as an additive into numerous materials and products including plastics, ceramics, glass, cement, rubber (e.g., car tires), lubricants, paints, ointments, adhesives, sealants, pigments, foods (as a source of Zn nutrient), batteries, ferrites, fire retardants, first aid tapes, etc. [8–10]. Recently, [11] have reported highly sensitive room temperature sensors based on the UV-LED activation of zinc oxide. So far, technological and engineering applications of ZnO usually require its dispersion in an organic phase. However, ZnO nanoparticles in aqueous media agglomerate into flocculates ranging from several hundred nanometers to several microns and thus do not interact with microorganisms effectively [12].

A main route for realizing the large-scale potential for polymer/ZnO nanocomposites is to homogeneously disperse ZnO with nanoscale dimension within the polymer matrix. Moreover, the control of the interfacial interactions is crucial, such that the ZnO crystalline phases remain stable within the composite.

According to a previous report [13], PEO exhibits a monoclinic crystalline order with cell parameters: $a = 8.05\text{Å}$, $b = 13.04\text{Å}$, $c = 19.48\text{Å}$, $\beta = 125.4^\circ$, forming a twisted linear chain of carbon and oxygen atoms

along the c axis. The twisted chains form $7/2$ helices (7 monomeric units turn around twice). On the other hand, ZnO crystallizes in the hexagonal wurtzite structure with space group $P6_3mc(c_{6n}^4)$, and the cell parameters under normal conditions of pressure and temperature are: $a = 3.253\text{Å}$ and $c = 5.2113\text{Å}$, according to the structure reported in the JCPDS 36-1451 file. This phase is stable in the temperature range between 20 to 100 °C [14].

Lee et al. [15] have examined the effects of the addition of ZnO powder on the mechanical, optical, and charge transport properties of a PEO-PVA-based polymeric complex. Lee also observed that high content of the ceramics filler rather deteriorates the composite properties due to particle agglomeration.

This paper presents a study of phase relationship of composite membranes prepared by embedding nanoparticles of ZnO in the PEO polymer matrix, using a solution-casting method. A simple and practical approach to prepare well-dispersed nanocomposites with ZnO nanoparticles in a poly (ethylene oxide) (PEO) matrix is demonstrated. The effect of ZnO content on the structures and properties of PEO-ZnO nanocomposites is studied by using X-ray diffraction, differential scanning calorimetry (DSC), Raman scattering, and impedance measurements.

2. EXPERIMENTAL

Poly(ethyleneoxide) (PEO, molecular weight 8,000,000 Aldrich) and zinc oxide (ZnO, Aldrich) were used without any further chemical purification. Anhydrous acetonitrile (Merck) was used as a solvent for the preparation of polymer as well as the polymer-ceramics composites. Required amounts of PEO and ZnO were dissolved separately in acetonitrile, obtaining solutions with concentrations of 2.5 and 5% wt. of the corresponding total solution weight, respectively, and each of them subject to ultrasound vibration for 45 min, and then mechanically stirred for 2.5 h. The two solutions were then mixed and stirred for 24 h until a homogenous mixture was obtained. The mixture was then poured into Teflon dishes (diameter 10 cm) and kept for evaporation inside a vacuum oven at 35 °C for 4 h followed by drying in desiccators under vacuum for 1 day. The final semitransparent, good quality, dry, free standing films had the following approximate

thickness: between 0.040 and 0.070 mm. Neat polymer composites were initially prepared with five different ZnO/PEO concentrations, x ($= 0, 5, 10, 20,$ and 30% wt. of total sample weight). For all concentrations of ZnO, good quality free standing polymer-ceramic composite films were obtained.

For conductivity measurements circular disc shaped samples (size: radius = 2.00 mm, thickness = 0.051 mm) were cut and then sandwiched between two stainless steel electrodes in a homebuilt cell using the two-electrode configuration. A K-type thermocouple located close to the sample was used as a temperature sensor. All the measurements were made in a nitrogen atmosphere. The temperature measurements were from 23 to 90 °C. The experimental temperatures were changed at intervals of 5 °C and the corresponding isotherm was maintained within ± 0.1 °C during each frequency-scan by the temperature-controlled shielded chamber. The impedance data, $Z(w) = \text{Re}Z(w) - i\text{Im}Z(w)$ ($i = \sqrt{-1}$, $w = 2\pi f[\text{Hz}]$) were collected, in the 10 - 32 MHz frequency range, using a Solartron 1260 impedance analyzer at a excitation signal of 500 mV.

Differential scanning calorimetry (DSC) measurements were done using a TA Instruments DSC Q100 in hermetically-sealed aluminum crucibles in the temperature range from 60 to 120 °C at a heating rate of 10°C/min for both heating and cooling cycle. X-ray diffraction measurements were done on an A8 Advance Buker AXS diffractometer, Cu-K α radiation from $5^\circ \leq 2\theta \leq 50^\circ$ at room temperature. Raman scattering spectra were recorded using a LabRam HR800 Horiba Jovin Yvon provided with an incident radiation source of 473 nm, and capabilities for measuring wave-number shift between 200 and 1400 cm^{-1} . The spectra were recorded in the 23–82°C temperature regions. The experimental temperatures were changed at intervals of 5 °C and the corresponding isotherm was maintained within ± 1.0 °C during each spectra-scan by a home-made temperature-controlled shielded chamber.

3. RESULTS AND DISCUSSION

3.1. X-ray diffraction (XRD) studies

Figure 1 shows the X-ray diffraction patterns of PEO, ZnO, and various PEO-ZnO composite samples at 25

°C. PEO shows major diffraction peaks at $2\theta = 19.2^\circ$ and 23.6° that correspond to the crystalline phase of the polymer [13]. ZnO shows a pattern whose main lines are indexed according to reported data, the JCPDS 36-1451 file. In the PEO–ZnO nanocomposites, the peaks of both components remain for all ZnO concentrations, without any appreciable change in peak positions or widths for those peaks assigned to the ZnO phase. Moreover, the PEO lines at 19.2° and 23.6° of the composites become greatly intensified compared to pure PEO, suggesting an increase in crystallinity.

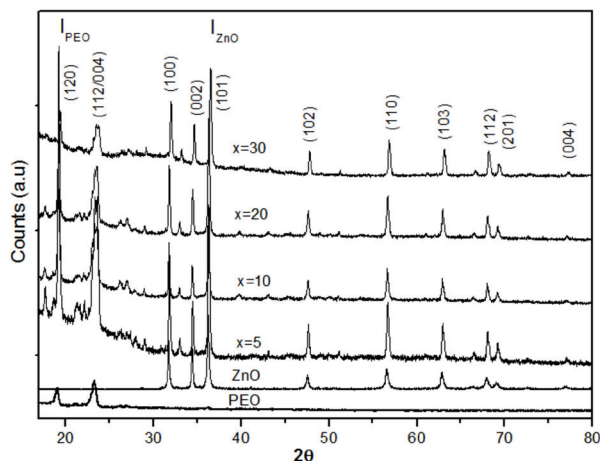


Figure 1. X-ray diffraction patterns of several PEO+xZnO composites. For comparison, the spectra of pure PEO and ZnO have also been reported. The peaks were indexed in accordance with [13] and [14] for PEO and ZnO, respectively. I_{PEO} and I_{ZnO} are control peaks for calculating the phase relationship.

The cell parameters for the various XRD patterns were fitted to the Xpovder program. In the case of the ZnO phase, the cell parameters were calculated from the evolution as a function of ZnO concentration of the (100), (002) and (101) reflexions, obtaining the values reported in Table 1, in which no major variations were observed in the composites compared with those of the PEO and ZnO crystalline phases [13,14,17]. Beyond that, an estimation of the average crystallite size of the dispersed ZnO nanoparticles, using the Debye-Scherrer's formula, gives 39 nm. Thus, these results

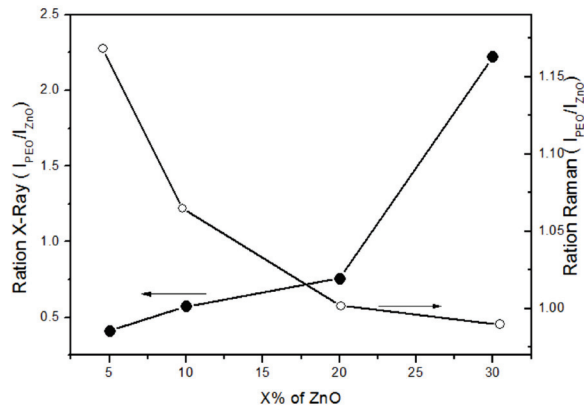


Figure 2. Plot of the ratio of $I_{\text{PEO}}/I_{\text{ZnO}}$ for both X-ray and Raman measurements as a function of ZnO content (x) at room temperature. The line is a visual guide.

indicate that the interaction between ZnO's oxygen ions and coordinating groups on PEO (O⁻) are very weak, resulting in two-phase composites for all ZnO concentrations. Even more, the two-phase composition of the membranes was monitored with the intensity ratio of the lines at $2\theta = 19.2^\circ$ (PEO) and $2\theta = 36.35^\circ$ (ZnO), respectively, as shown in Fig. 2. The intensity ratios $I_{\text{ZnO}}/I_{\text{PEO}}$ are in close agreement with the two-component weight ratio x .

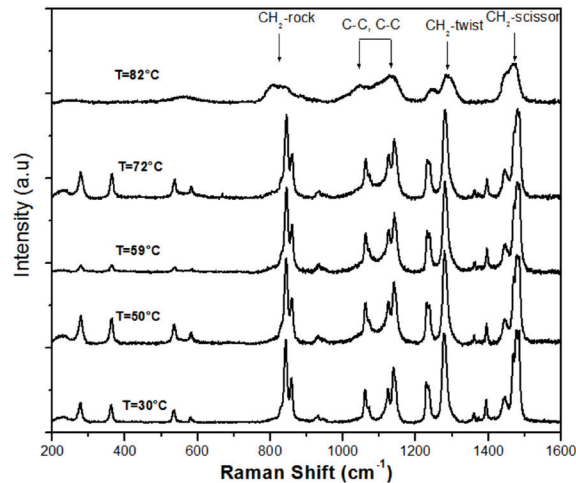


Figure 3. Variation with temperature of the Raman spectra of PEO. The peaks assignment was done according to [14].

3.2. Raman scattering (RS) studies

Figure 2 shows the Raman spectra of PEO at various isotherms in the 30–82 °C temperature range. The

assignment of bands corresponds to those reported in [16]. There are no marked changes in the characteristic bands for PEO; for example, in its $-\text{CH}_2$ rocking band near 839 cm^{-1} below approximately 70°C . However, the spectra recorded at 82°C show broadening and weakening (via normalization, not shown here) of all the signature PEO bands.

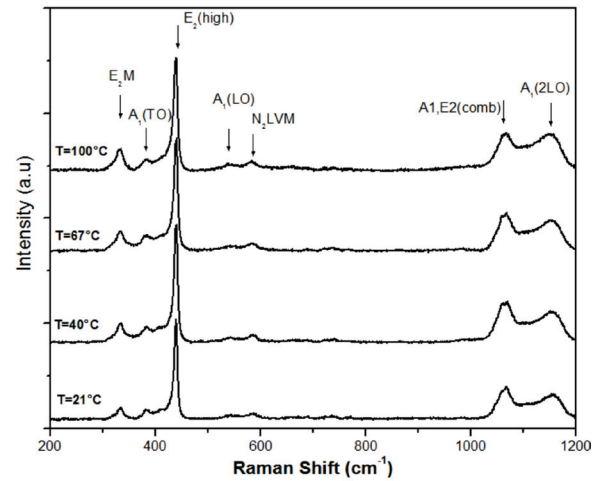


Figure 4. Variation with temperature of the Raman spectra of ZnO. The most intensive Raman line $E_2(\text{high})$ was assigned as a control peak to calculate phase relationship in the composites prepared.

Table 1. Structural parameters of the PEO+ x ZnO composite at 23°C

PEO+ x ZnO	PEO			ZnO		
	%	$a(\text{\AA})$	$b(\text{\AA})$	$c(\text{\AA})$	$a(\text{\AA})$	$c(\text{\AA})$
$X = 0$		8.021 ± 0.002	13.040 ± 0.007	19.484 ± 0.007		
$X = 5$		8.039 ± 0.007	13.0240 ± 0.005	19.451 ± 0.005	3.253	5.192
$X = 10$		8.027 ± 0.005	13.027 ± 0.007	19.089 ± 0.005	3.253	5.198
$X = 20$		8.019 ± 0.007	13.045 ± 0.009	19.590 ± 0.007	3.253	5.192
$X = 30$		8.023 ± 0.005	13.040 ± 0.008	19.364 ± 0.004	3.253	5.166
ZnO					3.253	5.204

Table 2. Calorimetric parameters of the PEO+ x ZnO composite

PEO+ x ZnO	$T_m(^{\circ}\text{C})$	$D\Delta_m(\text{J/g})$	$c(\%)$
$X = 0$	66.2	175.9	100
$X = 5$	64.8	166.7	94.7

PEO+xZnO	$T_m(^{\circ}C)$	$D\Delta_m(J/g)$	$c(\%)$
X = 10	65.5	138.5	78.7
X = 20	65.3	141.5	80.4
X = 30	66.5	126.7	72.0

with respect to those shown at room temperature spectra, thus indicating higher local disorder. For the region with a wave-number less than 1000 cm^{-1} , the existing bands are associated with distortion in the $-CH_2$ groups ($-CH_2$ rocking bands), while those in the region with a wave-number greater than 1000 cm^{-1} are associated with vibrations in the C-O, C-C and $-CH_2$ bonds. When PEO is heated through its melting point, those vibrational modes with lowest wave-numbers are susceptible to disappear, while those with higher wave numbers tend to overlap each other, forming broader bands, which is characteristic of an amorphous material.

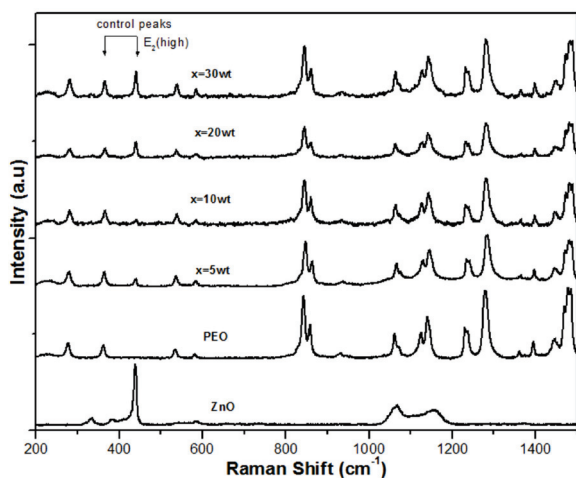


Figure 5. Micro-Raman spectra of the composites recorded at 25 °C. Arrows indicate the control peaks used to calculate the two-phase mixture composition.

Figure 4 shows the Raman spectra of ZnO at various temperatures between 21 and 100 °C without any appreciable variations among them, in concordance with the reports [14]. The band assignments are identical to those previously reported [14]. The Raman active peak designated as $E_2(\text{high})$ was chosen as the most representative one for further analysis of the spectra. This peak at around 420 cm^{-1} is basically attributable to non-polar phonon vibrations of the ZnO structure according to previous results [17,18] and is characteristic of a hexagonal-crystalline structure, in concordance with the XRD results.

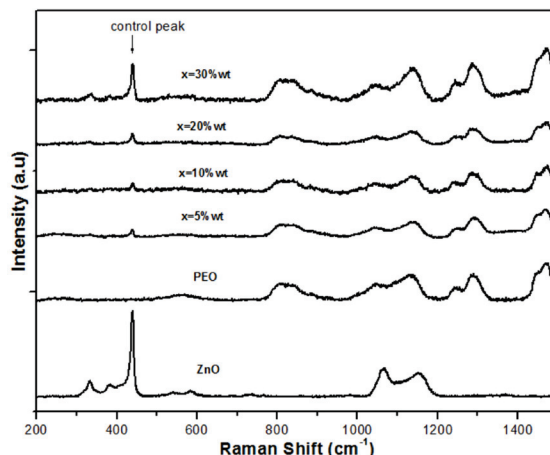


Figure 6. Micro-Raman spectra of the composites, recorded at 70 °C. The arrow indicates the control peak used to calculate the two-phase mixture compositions.

Figure 5 shows the Raman spectra of pure PEO, ZnO, and various PEO-ZnO composites at 25 °C. In the PEO-ZnO nanocomposites, the Raman modes of each individual component remain for all ZnO concentrations, without no appreciable change in peak positions or widths for those peaks assigned to the pure components. The Raman results are consistent with the XRD results, indicating that the interaction between the PEO and ZnO crystalline phases is probably weak. Figure 6 shows the Raman spectra obtained at 70 °C, close to the melting point of PEO, where the peaks attributed to PEO become broader, showing a decrease in the crystallinity of the polymer phase. On the other hand, those modes attributed to the filler remain unalterable, indicating that no interactions between the polymer chain and the ZnO nanoparticles are taking place. Moreover, as in the case of the of the XRD analysis, the two-phase composition of the membranes was monitored with the intensity ratio of the Raman peaks I_{PEO} and I_{ZnO} , respectively, as indicated in Fig. 2. The Raman results confirm again that the intensity ratios I_{ZnO}/I_{PEO} are in close agreement with the two-component weight ratio, x .

3.3. Differential scanning calorimetry (DSC) studies

DSC results for the PEO-ZnO composites at various concentrations (not shown) indicated that the melting point of the PEO crystalline phase is almost the same as that observed for pure PEO whose melting endothermic is observed at around 60 °C, implying a conservation

in the degree of crystallinity compared to that of pure PEO. That is, the DSC results are consistent with the structural results reported above, in the sense that the addition of the ZnO nanoparticles does not seem to affect the

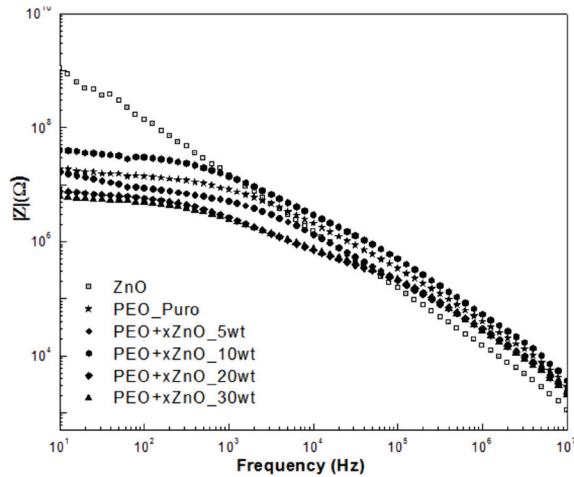


Figure 7. The Bode plots, impedance modulus vs. frequency, for various composites at 50 °C

crystalline phase of PEO, as a consequence of none or very weak interaction between the added ZnO nanoparticles.

3.4. Impedance spectroscopy (IS) studies

The frequency dependence of the impedance, plotted as $\log |Z|$ vs. $\log f$, for pure PEO, ZnO, and the PEO-ZnO composites, is shown in Fig. 7 for the data collected at 50 °C; and Fig. 8, for the impedance data collected at 90 °C. All the Nyquist plots, $-\text{Im}Z$ vs. $\text{Re}Z$ (not shown), in the tested frequency range from 10 to 10 MHz, gave a semicircle that is well modeled by an equivalent circuit consisting of a parallel combination of a capacitance (C) and a resistance (R). The value of the resistance is very high for pure ZnO, so its impedance behaves as $-i/2\pi fC$, and therefore, $|Z|$ is proportional to $1/f$, as shown in Figs. 8 and 9. On the other hand, PEO showed a lower resistance than ZnO, and therefore an almost flat region is exhibited in the low-frequency range, where the capacitive reactance is much higher than the resistive one, thus $|Z|$ is dominated by R as shown in Figs. 7 and 8.

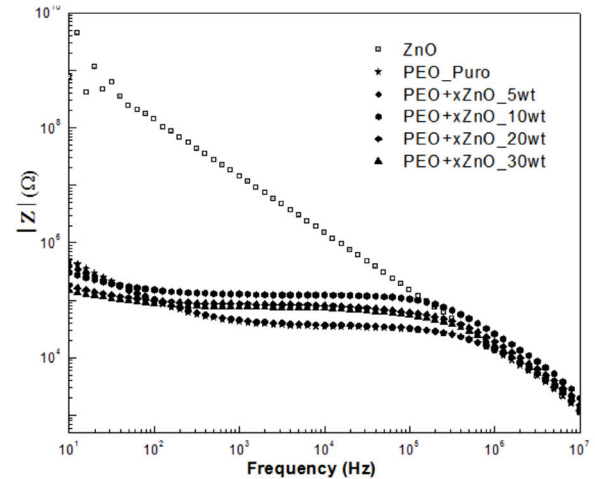


Figure 8. The Bode plots, impedance modulus vs. frequency, for various composites at 90 °C

4. CONCLUSION

In this contribution we have successfully demonstrated the benefits of introducing highly-dispersed ZnO with nanoscale dimension within the PEO matrix. The composites were characterized by XRD, Raman scattering, DSC and impedance spectroscopy analysis. The results indicate that the control of the interfacial interactions is crucial, such that the ZnO crystalline phases remain stable within the nanocomposites. In particular, the XRD and Raman scattering results show more defined peaks assigned to each phase of the composite as the ZnO content increases from 0 to 30 % weight ratio, thus indicating that ceramic filler remain in the semi-crystalline polymer matrix as a separate crystalline phase, or that the interaction between the PEO and ZnO crystalline phases is probably weak, even above the melting point of the PEO crystalline phase. In addition, the DSC results are consistent with the XRD and RS results, in the sense that the addition of the ZnO nanoparticles do not seem to affect the crystalline phase of PEO. The dc-electrical conductivity of the composites slightly increases with ZnO content, reaching a value of the order of 10^{-5} Scm^{-1} at 90 °C.

ACKNOWLEDGEMENTS

The authors wish to acknowledge the support of DIMA (*Dirección de Investigación, Universidad Nacional de Colombia, Sede Manizales*) given to the research project.

REFERENCES

- [1] Klingshir, C., Review article: ZnO: from basics towards applications, *Phys. Status sold. B-Basic Solid State physics*, 244, pp. 3019-3023, 2007.
- [2] Armand, M. B., Chabagno, J. M., Duclot, M., Polyethers as solid electrolytes. In *Fast Ion Transport in Solids*; Vashishta P., Mundy J.N., Shenoy G.K., Eds.; Elsevier North-Holland, Inc.: Amsterdam, 1979.
- [3] Caruso, T., Capoleoni, S., Cazzanelli, E., Agostino, R.G. and Villano, P. et al., Characterization of PEO_Lithium triflate polymer electrolytes conductivity, DSC and Raman investigations, *Ionics* 8, pp. 36-43, 2002.
- [4] Ayala, G., Agudelo, A., Vargas, R., Efecto del glicerol sobre las propiedades eléctricas y comportamiento de fase en biopolímeros de almidón de yuca, *Dyna*, 171, pp. 138-147, 2012.
- [5] Hema, M., Selvasekerapandian, S., Hirankumar, G., Sakunthala, A., Arunkumar, D., et al., Structural and thermal studies of PVA:NH₄I, *J. Phys. Chem. Solids*, 70, pp. 1098-1103, 2009.
- [6] Huchen, Z., Jianji, W., Honghe, Z., Kelei, Z. and Yang, Z., Interactions of nanosized Al₂O₃ and ZnO with poly(ethylene)oxide-NaSCN polymer electrolytes, *J. Phys. Chem. B*, 109, pp. 2610-2616, 2005.
- [7] Bambang, V., Jae-D, K., Byoung K., Young, H., Youn-W, L., et al., *The Journal of Supercritical Fluids*, 52(1), pp.76-83, 2010.
- [8] Hernández, A., González, R., Viesca, J.L., Fernández, J.E., Fernandez, J.M., et al., CuO, ZrO₂ and nanoparticles as antiwear additive in oil lubricants, *Wear*. 265(3-4), pp. 422-428, 2008.
- [9] Turkovic, A., Crnjak, Z., Orel, N., Dean, F., Vibrational study of the crystalline phase in (PEO)₈ZnCl₂ nanocomposite electrolyte, *Vacuum* 80, pp. 208-212, 2005.
- [10] Klingshirn, C., ZnO: From basics towards applications, *Physica Status Solidi B*, 244, pp. 3027–3073, 2007.
- [11] Costello, B.P.J., Ewen, R.J., Ratcliffe, M.N. and Richards, M., Highly sensitive room temperature sensor based on the UV-LED activation of zinc oxide, *Sensors and Actuators B*, 134, pp. 945-952, 2008.
- [12] Gordon, A., Benny, P., Ofir, H., Oubara, I.F., Ehud B., et al., Synthesis and characterization of zinc/iron oxide composite nanoparticles and their antibacterial properties *Colloids and Surfaces A: Physicochem. Eng. Aspects*, 374, pp.1–8, 2011.
- [13] Kuila T., Acharya, H., Srivastava, S.K., Samantaray, B.K., Kureti, S., Enhancing the ionics conductivity of PEO based plasticized composite polymer electrolyte by LaMnO₃ nanofiller, *Mater. Sci. Eng., B* 137, pp. 217-224, 2007.
- [14] Carlos, V.-H., Francly, N.J., and Jesús, F.J., Películas de ZnO impurificadas con MnO usando la técnica SILAR, *S. Revista Latinoamericana de Metalurgia y Materiales*, S1(2), pp. 501-506, 2009.
- [15] Lee, J., Bhattacharyya, D., Easteal, A.J., Metson, J.B., Properties of nano-ZnO/poly(vinyl alcohol)/poly(ethylene oxide) composite thin films, *Current Applied Physics*, 8, pp. 42-47, 2008.
- [16] Roger, F. and Weiwei, H., Conformational changes in diethylene glycol dimethyl ether and poly(ethylene oxide) induce by lithium ion complexation, *Macromoleculas*, 28, pp. 1246-1251, 1995.
- [17] Liming, S., Ningzhong, B., Kazumichi, Y., Kazunuri, D., Arunava, G., et al., Direct synthesis of ZnO nanoparticles by solutions-free mechanochemical reaction, *Nanotechnology*, 17, pp. 5117-5120, 2006.
- [18] Damen, T.C., Porto, S.P., Tell B., Raman effect in Zinc oxide, *Phys. Rev.*, 142, pp. 570-574, 1966.